RESEARCH ARTICLE | OCTOBER 08 2024

Contribution of rolling resistance to the drag coefficient of spheres freely rolling on a rough inclined surface

S. D. J. S. Nanayakkara ✉ iD ; S. J. Terrington iD ; J. Zhao iD ; M. C. Thompson iD ; K. Hourigan iD

Check for updates

View Online   Export Citation

Articles You May Be Interested In

Transition to chaos in the wake of a circular cylinder near a moving wall at low Reynolds numbers

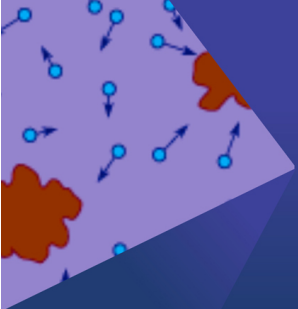*Physics of Fluids* (September 2020)

A deep learning approach to classifying flow-induced vibration response regimes of an elliptical cylinder

Physics of Fluids (April 2024)

Simultaneous measurements of time-resolved velocity and concentration fields behind a sand dune-inspired jet in crossflow

Physics of Fluids (November 2021)

Physics of Fluids

Special Topic:

250 Years of Brownian Motion

Guest Editors: Alan Jeffrey Giacomin and Nhan Phan-Thien

Submit Today!

AIP Publishing

AIP Publishing

Contribution of rolling resistance to the drag coefficient of spheres freely rolling on a rough inclined surface

View Online   Export Citation   CrossMark

S. D. J. S. Nanayakkara,[1,a] (iD) S. J. Terrington,[1] (iD) J. Zhao,[1,2] (iD) M. C. Thompson,[1] (iD) and K. Hourigan[1] (iD)

AFFILIATIONS

[1]FLAIR, Department of Mechanical and Aerospace Engineering, Monash University, Clayton, VIC 3800, Australia
[2]School of Engineering and Technology, University of New South Wales, Canberra ACT 2610, Australia

[a]Author to whom correspondence should be addressed: sheran.nanayakkara@monash.edu

ABSTRACT

The drag coefficient (C_D) of a sphere freely rolling without slipping on a rough plane is presented in this study. Increasing panel roughness has been found to increase C_D, although lubrication theory predicts that the larger gap imposed by the rougher panel should yield a smaller drag. We propose that this increase in drag is due to the effects of rolling resistance, which increases with panel roughness. The total drag on a sphere is decomposed into fluid drag and drag due to rolling resistance, where the fluid drag is predicted using a combined analytical–numerical approach. It is shown that rolling resistance can be modeled as a resistive torque opposing the sphere motion, generated by the offset contact normal force from the sphere center plane. This coefficient of rolling resistance (μ_r) can be predicted using the root mean square roughness (R_q) of the panel. Additionally, μ_r is observed to increase with sphere down-slope velocity and an empirical relationship between μ_r, R_q, and non-dimensional velocity (U^*) is given. A comparison of the drag predicted by the proposed model with measured data indicates good agreement for all the four panels considered. Consistent with previous literature, a non-linear relationship between μ_r, R_q, and U^* is proposed. Although increasing panel roughness leads to a smaller fluid drag due to the larger gap imposed by rougher panels, the drag due to rolling resistance increases more rapidly. This leads to an increase in total drag with increase in the panel roughness. Additionally, increasing panel roughness is observed to have a significant effect on the sphere wake, leading to irregular wake shedding and increase in the Strouhal number.

I. INTRODUCTION

The motion of small spherical particles in a viscous fluid at low to moderate Reynolds numbers represents one of the earliest categories of problems investigated in fundamental fluid mechanics. Reinforcing its historical significance, the hydrodynamic interactions between particles and walls continue to be a subject of interest (Thompson *et al.*, 2021). These interactions play a crucial role in various applications, such as separation techniques in analytical chemistry, biological flows, movement of undersea vehicles, rock movements in debris flow, leukocyte rolling, and sediment transport. Other related applications include the handling, pumping, and storage of particulate materials, surface cleaning, submarine dredging as well as modeling of ball bearings and hydroplaning of underwater landslides (Thompson *et al.*, 2021). A simple example of this problem is the prediction and modeling of the transport of sediments under the action of waves or underwater landslides in rivers and seabed, based on bed characteristics. The focus of this article is to explore the hydrodynamic interactions between a particle and a rough wall at low to moderate Reynolds numbers.

A sphere immersed in a fluid that rolls down a plane wall without slipping has been extensively studied as a canonical example of particle–wall interactions (Carty, 1957; Goldman *et al.*, 1967; and Thompson *et al.*, 2021). At low to moderate Reynolds numbers ($Re = UD/\nu$), the drag coefficient (C_D) has been found to decrease as the combined amplitude of surface roughness of the sphere and wall increases (Nanayakkara *et al.*, 2024b). A similar observation was made for cylinders rolling on a wall (Nanayakkara *et al.*, 2024a). Surface roughness introduces an effective hydrodynamic gap between the sphere and the wall (Houdroge *et al.*, 2023; Galvin *et al.*, 2001; Zhao

15 October 2024 06:34:02

et al., 2002; Smart and Leighton, 1989; Smart *et al.*, 1993; and King and Leighton, 1997). As the surface roughness is increased, the imposed gap height increases, which results in a decrease in the magnitude of pressure in the gap where lubrication forces dominate, leading to a decrease in hydrodynamic drag (Houdroge *et al.*, 2023; Nanayakkara *et al.*, 2024b). However, many previous studies on the rolling sphere problem have considered relatively smooth surfaces. When the panel surfaces are significantly rougher than the sphere surfaces (by a factor of 10 or more), C_D is found to increase with surface roughness (Jan and Shen, 1995; Jan and Chen, 1997; and Garde and Sethuraman, 1969) in contrast with the predicted decreasing hydrodynamic drag. This is likely a result of increased rolling resistance with increasing surface roughness, which we will explore in the present study. This study follows on from the previous study by the same authors (Nanayakkara *et al.*, 2024b), where the effects of surface roughness on the drag coefficient of spheres freely rolling on a relatively smooth inclined plane were discussed. The planes considered here are significantly rougher (10–100 times) than those investigated in Nanayakkara *et al.* (2024b). For the smoother panels in Nanayakkara *et al.* (2024b), the effects of rolling resistance were small and the drag coefficient was observed to decrease with increasing panel roughness. The larger roughness of the panels investigated in this study introduces significant rolling resistance, which increases with increasing panel roughness.

Jan and Shen (1995) investigated the effects of rolling resistance on the drag coefficient of a rolling sphere and found that the drag was approximately 1.3 times higher for the simulated rough boundary. They obtained expressions for the rolling resistance of a sphere on a rough boundary by using an energy balance approach. They suggest that rolling resistance is composed of two mechanisms, collisions with roughness elements and friction; the combined rolling resistance and drag coefficients were determined empirically using linear regression. Jan and Chen (1997) also proposed that rolling resistance arises due to a combination of collisions and sliding friction force, where both coefficients are to be determined empirically. Garde and Sethuraman (1969) conducted similar experiments for an artificial rough boundary and found the drag coefficient to be larger for the rough boundary than for the smooth boundary. Significant scatter was observed for the rough boundary data, although the general underlying $1/\text{Re}$ trend was observed. They found an increase in rolling resistance with a reduction in Re and attributed the longer contact between sphere and roughness elements at lower speeds to this observed increase in rolling resistance. Additionally, a reduction in rolling resistance was observed for an increase in the ratio D/K (sphere diameter/diameter of roughness element). Jan and Chen (1997) also observed a similar decreasing trend of friction coefficients with increasing D/K. This implies that for a fixed roughness element size, the increase in sphere diameter results in a smaller rolling resistance coefficient.

Zhao *et al.* (2002) considered the motion of a sphere down an inclined plane containing a sparse distribution of large asperities with smaller asperities between the larger ones. Their model included the lubrication forces opposing the liftoff and settling motion when larger asperities are encountered while also allowing for sphere slippage. However, a constant coefficient of static friction and sliding friction was assumed in their analysis and the relationship between roughness and rolling resistance was not investigated.

Although rolling resistance has been attributed as a primary mechanism responsible for the observed increase in drag coefficient for rougher boundaries, the present literature lacks a detailed quantitative investigation into the relationship between how surface roughness affects the rolling resistance and drag coefficient of rolling spheres. The aim of the present article is to investigate the relationship between surface roughness on the combined effects of hydrodynamic drag and rolling resistance on the motion of a sphere rolling without slipping on a rough wall.

A. Rolling resistance

The study of the nature of friction and rolling resistance appears to be first documented by Leonardo da Vinci using wooden balls as the rolling element in bearings (Hutchings, 2023), which was later investigated experimentally by de Coulomb using wooden cylinders rolling on wooden surfaces. Numerous research articles have been published on this subject, including foundational work by Tabor (1955). Recent studies have focused on automotive applications (Sun *et al.*, 2024) and particulate systems (Ai *et al.*, 2011). However, a complete analytical model that predicts the rolling resistance of a sphere of a known diameter rolling on a surface with known physical parameters, such as surface roughness, is yet to be developed. As is typically done with friction studies, rolling resistance is evaluated experimentally using empirical data.

As a sphere rolls on a surface, any mechanism that causes asymmetry of the forces at the area of contact leads to a resistance torque that opposes sphere motion (Wilson *et al.*, 2017). The diverse mechanisms contributing to energy dissipation, collectively referred to as rolling resistance (sometimes as rolling friction), have been previously discussed in the literature (Bikerman, 1949; Halling, 1958). Some notable mechanisms include surface roughness, shape effects, viscoelastic dissipation, hysteresis effects, interfacial slip, molecular adhesion, and capillary action. Section VI discusses some of the mechanisms in detail. As will be discussed in Sec. II, for hard spheres rolling on a hard surface, surface roughness is the most likely source of rolling resistance under the experimental conditions discussed in the present study.

The relationship between surface roughness and rolling resistance has been explored by many authors for spheres and cylinders under varied conditions. Bikerman (1949) investigated the minimum tilt angle required by ball bearings to roll down stainless steel panels with varied surface finishes. Their results showed an approximate correlation between the predicted height of asperities with the measured surface asperities, assuming that rolling resistance is due to the sphere having to overcome these asperities. Better agreement was obtained for rougher surface finishes, while the surfaces with a smoother finish diverged from predictions. Halling (1958) investigated the dependence of rolling resistance on surface texture for unloaded and loaded steel rollers on machined steel plates. An increasing coefficient of rolling resistance μ_r with increasing centerline average roughness was observed.

Cross (2015) investigated the effects of surface roughness on μ_r of hard steel spheres rolling on hard surfaces in the air by varying the surface roughness of the panel using emery paper. Cross (2015) discovered that μ_r increases with sphere velocity and panel roughness and decreases with sphere diameter. Based on these results, Cross (2016) developed an analytical model relating μ_r to the height of roughness asperities (r), velocity (U), and sphere diameter (D) by considering the energy loss during a collision between a surface asperity and the wall, with coefficient of restitution (e_y),

$$\mu_r = \frac{(1 - e_y^2)NU^2 r}{0.7\pi g D^2}, \qquad (1)$$

where N is the number of collisions per revolution. Experimentally, Cross (2016) found that $\mu_r \propto U$, indicating that N may be inversely proportional to U. Additionally, Cross (2016) also found that $\mu_r \propto 1/D^{1-1.7}$, indicating that N and e_y also vary with D. Therefore, Eq. (1) is not perfectly able to capture the dependence of μ_r on U and D. Dimensional analysis suggests that the coefficient of rolling resistance takes the following form:

$$\mu_r = a\left(\frac{r}{D}\right)^b \left(\frac{U}{\sqrt{gD}}\right)^c, \qquad (2)$$

with coefficients a, b, and c to be determined experimentally. Note that we expect these coefficients to differ from the experiments of Cross (2016) since they consider vastly different experimental conditions (steel spheres in air vs acrylic spheres in water).

Wilson *et al.* (2017) also proposed a model for the rolling resistance coefficient of a rough sphere rolling on a plane wall. They considered the viscoelastic energy loss due to the deformation of surface asperities as the sphere rolls and obtained the following expression for the resistive torque applied to the sphere:

$$\tau_{decel} = 2\hat{\xi}\eta_n d_t^2 n_{2\pi} \frac{U}{D/2}, \qquad (3)$$

where $\hat{\xi}$ is a parameter to be determined empirically, η_n is the damping coefficient that characterizes incomplete restitution of the velocity during normal contact, d_t is the tangential distance from each contact point to the center of mass, and $n_{2\pi}$ is the number of expected contacts over one revolution. We note, however, that the parameter $\hat{\xi}$ may vary with respect to some of the other parameters, which requires empirical fitting of the model to experimental results. Therefore, the present study assumes the rolling resistance coefficient is of the form shown in Eq. (2), and the coefficients a, b, and c are obtained experimentally.

In this study, we will experimentally investigate the relationship between surface roughness and the combined effects of hydrodynamic drag coefficient ($C_{D,f}$) and coefficient of rolling resistance (μ_r) of spheres freely rolling without slipping on an inclined rough plane. We propose a model similar to those of Cross (2016) and Wilson *et al.* (2017), with a power-law dependence on surface roughness and sphere velocity. The hydrodynamic drag coefficient is estimated using the relationship between surface roughness and gap height required by lubrication theory as described in Nanayakkara *et al.* (2024b). A new model that describes μ_r in terms of the root mean square roughness (R_q) and non-dimensional down-slope velocity (U^*) is proposed, with constants of proportionality to be determined empirically.

This paper is organized as follows. Section II describes the problem and the analytical–numerical solutions that describe the hydrodynamic drag. Section III presents the new empirical model that describes the coefficient of rolling resistance of a sphere. Section IV presents a description of the experimental setup and method. Section V presents detailed experimental results of the investigation together with a discussion of the results. Section VI briefly discusses additional sources of rolling resistance, while Sec. VII presents flow visualizations highlighting the influence of surface roughness on the wake of a rolling sphere. Concluding remarks are given Sec. VIII.
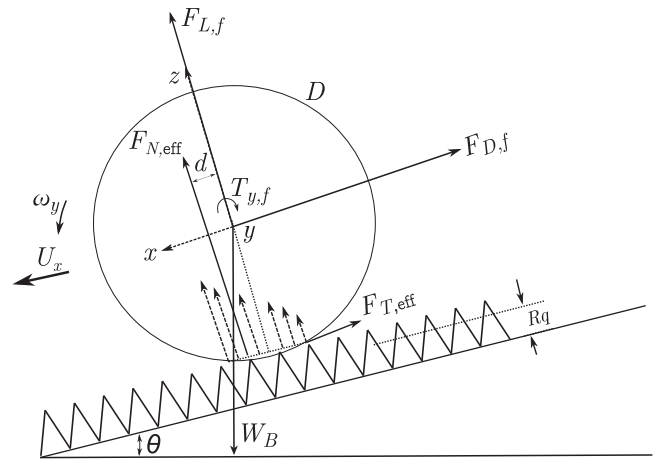

FIG. 1. Schematic free body diagram of the forces acting on a sphere rolling down an inclined plane under the influence of gravity, in a stationary fluid.

II. PROBLEM DESCRIPTION

This investigation focuses on the motion of a sphere with diameter D immersed in an initially stationary fluid and which rolls without slipping down a rough plane inclined at an angle (θ) relative to the horizontal, as depicted in Fig. 1. The sphere has a density ρ_s, while the fluid has a density ρ_f; typically, the sphere is denser than the fluid ($\rho_s > \rho_f$, negatively buoyant). We consider a Cartesian coordinate system (x, y, z) fixed to the sphere's center.

The sphere travels down the inclined plane with instantaneous translational and rotational velocities $U_x = U$ and $\omega_y = \omega$, respectively. The forces and torques acting on the sphere include the buoyant weight $W_B = \pi g D^3(\rho_s - \rho_f)/6$, the hydrodynamic drag ($F_{D,f}$), lift ($F_{L,f}$) and torque ($T_{y,f}$), and the normal ($F_{N,\text{eff}}$) and tangential contact forces ($F_{T,\text{eff}}$). The total force resisting the motion includes both the hydrodynamic drag and the tangential contact force, $F_{D,\text{Total}} = F_{D,f} + F_{T,\text{eff}}$.

The rolling sphere reaches a quasi-steady state, with time-mean velocity $\overline{U}$ and angular velocity $\overline{\omega}$. The time-mean Reynolds number is given by $\overline{Re} = \overline{U}D/\nu$. Time-averaged forces are expressed as $\overline{F}_{D,f}, \overline{F}_{L,f}, \overline{T}_{y,f}, \overline{F}_{N,\text{eff}}, \overline{F}_{T,\text{eff}}$, and $\overline{F}_{D,\text{Total}}$. Force balance parallel to the plane gives:

$$\overline{F}_{D,\text{Total}} = \overline{F}_{D,f} + \overline{F}_{T,\text{eff}} = W_B g \sin\theta. \qquad (4)$$

As such, we obtain the following expression for the time-averaged total drag coefficient:

$$\overline{C}_{D,\text{exp}} = \frac{\overline{F}_{D,\text{Total}}}{\frac{1}{8}\pi D^2 \rho_f \overline{U}^2} = \frac{W_B g \sin\theta}{\frac{1}{8}\pi D^2 \rho_f \overline{U}^2} = \frac{4g\sin(\theta)D(\beta-1)}{3\overline{U}^2}. \qquad (5)$$

We assume that the sphere makes contact with the plane via surface asperities with an unknown number of contact points and corresponding reaction forces as shown in Fig. 1. Due to uneven contact pressure distribution across the contact area, the effective time-averaged normal contact force $\overline{F}_{N,\text{eff}}$ is offset from the sphere's center of mass by a distance d. Then, the balance of time-averaged torques about the sphere is

$$\overline{T}_{Y,f} + \overline{F}_{N,\text{eff}}d - \overline{F}_{T,\text{eff}}D/2 = 0. \qquad (6)$$

The total time-averaged resistance force parallel to the plane can be expressed as

$$\overline{F}_{D,\text{Total}} = \overline{F}_{D,\text{f}} + \overline{F}_{T,\text{eff}}, \tag{7}$$

and substituting (6) in Eq. (7) yields

$$\overline{F}_{D,\text{Total}} = \overline{F}_{D,\text{f}} + \frac{\overline{T}_{Y,\text{f}}}{D/2} + \frac{\overline{F}_{N,\text{eff}}d}{D/2}. \tag{8}$$

The term $\overline{F}_{D,\text{f}}$ is the fluid drag contribution to the total drag, while the term $\overline{T}_{Y,\text{f}}/(D/2)$ describes the tangential contact force required to oppose the fluid torque and maintain the no-slip condition. Finally, the term $\overline{F}_{N,\text{eff}}d/(D/2)$ represents the effects of rolling resistance.

The first two terms in Eq. (8) are combined into an effective fluid drag force,

$$\overline{F}_{D,\text{f,eff}} = \overline{F}_{D,\text{f}} + \frac{\overline{T}_{Y,\text{f}}}{D/2}, \tag{9}$$

which is the drag force obtained in the absence of rolling resistance. This effective drag includes the part of the tangential contact force required to oppose the fluid torque, in addition to the fluid drag.

Houdroge *et al.* (2023) obtain the following expression for the effective drag coefficient, assuming both a smooth sphere and a smooth wall and assuming a small gap G exists between the sphere and the wall:

$$\overline{C}_{D,\text{f,eff}} = \frac{1}{Re}\left[-44.2\log_{10}(G/D) + 34.0\right]$$
$$+ \left[1.70 - 0.136(\log_{10}Re) - 0.0716(\log_{10}Re)^2\right]. \tag{10}$$

This expression was obtained by combining the predictions of lubrication theory with numerical simulations. The total drag was assumed to include both a gap-drag term and a gap-independent wake-drag term. The gap-drag was determined analytically, using the theory of lubrication (Goldman *et al.*, 1967), while the wake drag was obtained using numerical simulations. Equation (10) was then obtained by empirically fitting the numerical data over the range $5 < \text{Re} < 300$ (Houdroge *et al.*, 2023).

A recent experimental investigation conducted by Nanayakkara *et al.* (2024b) found excellent agreement between experimental results and Eq. (10) when G was assumed to be the same order as the combined R_q roughness of the sphere and panel. Physically, it is assumed that surface roughness introduces an effective hydrodynamic gap between the sphere and the wall, approximately equal to R_q. Note that (10) is obtained under the assumption $d = 0$ and therefore does not include any rolling resistance. This was found to be accurate for the generally smooth glass panels discussed in Nanayakkara *et al.* (2024b).

The third term in Eq. (8), $\overline{F}_{N,\text{eff}}d/(D/2)$, describes the resistive torque that opposes the sphere's motion, due to the normal reaction force being offset ahead of the sphere's center of mass (Cross, 2016; Sharma and Reid, 1999; Wilson *et al.*, 2017; and Halling, 1958). This results in an effective rolling resistance force,

$$\overline{F}_{\text{rr}} = \frac{d}{D/2}\overline{F}_{N,\text{eff}} = \mu_r\overline{F}_{N,\text{eff}}, \tag{11}$$

where $\overline{F}_{N,\text{eff}} = W_Bg\cos(\theta) - \overline{F}_L$ from Fig. 1 and $\mu_r = d/(D/2)$ is the coefficient of rolling resistance that is commonly used in the literature (Wilson *et al.*, 2017; Cross, 2016).

Houdroge *et al.* (2023) predicted numerically the lift coefficient of a freely rolling sphere to be in the range $-0.7 \leq \overline{C}_L \leq 0.2$ for $\overline{Re}$ in the range $0.1 \leq \overline{Re} \leq 200$, which is small compared to the normal component of the buoyant weight, $10 \leq W_Bg\cos(\theta)/\frac{1}{8}\pi D^2\rho_f\overline{U}^2 \leq 165$; as such, $\overline{F}_L$ can be assumed to be negligible.

Then, the contribution of rolling resistance to the drag coefficient is defined as

$$\overline{C}_{D,\text{rr}} = \frac{d}{D/2}\frac{W_Bg\cos(\theta)}{\frac{1}{8}\pi D^2\rho_f\overline{U}^2} = \mu_r\frac{4D(\beta - 1)g\cos(\theta)}{3\overline{U}^2}. \tag{12}$$

Equation (12) describes the contribution of rolling resistance to the total drag coefficient, in terms of μ_r. We propose that μ_r will depend on surface roughness and sphere velocity. Sections III and V C will elaborate further on this proposed relationship.

Finally, combining (10) and (12), we obtain the following expression for the total predicted time-mean drag coefficient of a freely rolling sphere:

$$\overline{C}_{D,\text{pred}} = \overline{C}_{D,\text{f,eff}} + \overline{C}_{D,\text{rr}}, \tag{13}$$

where the coefficient of rolling resistance μ_r is the only unknown parameter.

III. ROLLING RESISTANCE MODEL

A primary aim of the present investigation is to establish the relationship between μ_r to be used in Eq. (12) and various surface roughness parameters. In Nanayakkara *et al.* (2024b), it was shown that R_q was a good approximation for G. Similarly, it is proposed that R_q is a suitable roughness parameter that can be used to describe μ_r. Additionally, the experimental and numerical investigations conducted by Cross (2016) and Wilson *et al.* (2017), respectively, have determined that μ_r is a function of the sphere velocity and diameter. To incorporate this velocity and diameter dependence of μ_r, we will introduce a new non-dimensional velocity as follows:

$$U^* = \overline{U}/\sqrt{Dg}. \tag{14}$$

This non-dimensional velocity was obtained by applying dimensional analysis to the model of Cross (2016) for the rolling resistance of a rough sphere. Furthermore, the relationship between U^* and $\overline{Re}$ can be expressed as

$$\overline{Re} = U^*D^{1.5}g^{0.5}/\nu. \tag{15}$$

As such, we propose the following relationship between μ_r with U^* and non-dimensional roughness ξ_q:

$$\mu_r = a \times (\xi_q)^b \times (U^*)^c. \tag{16}$$

Here, a, b, and c are constants to be determined empirically.

We can also rewrite (12) in terms of U^* as

$$\overline{C}_{D,rr} = \mu_r\frac{4(\beta - 1)\cos\theta}{3(U^*)^2}. \tag{17}$$

It should be noted that the proposed simple empirical model in Eq. (16) is only first-order accurate. Given that the roughness characteristics of real surfaces are complex and display many scales in both amplitude and spacing, the use of a simple parameter such as R_q will not effectively capture all aspects of the surface. Furthermore, a sphere

moving down an inclined plane exhibits a cross-slope velocity component [see Nanayakkara *et al.* (2024b) for further details], which is also likely to influence μ_r. However, (16) provides an approximate solution to the complex problem of estimating the rolling resistance of a sphere using simple parameters that will be useful when predicting the drag on a freely rolling sphere.

IV. EXPERIMENTAL SETUP AND METHODOLOGY

The experiments using rolling spheres were conducted in the Fluids Laboratory for Aeronautical and Industrial Research (FLAIR) at Monash University. A detailed explanation of the experimental setup and methodology used in this study can be found in Nanayakkara *et al.* (2024b). A brief summary is given below.

A. Summary of experimental setup and methodology

The experiments were carried out in a water tank with a glass panel mounted on an adjustable stainless steel frame. The inclination angle was varied from 4° to 23°. Additionally, various test panels with different surface roughness levels were used. Before the experiments, the spheres were presoaked underwater, with air bubbles removed through vibration and stirring. Subsequently, the spheres were gently released onto a collection port on the plane to minimize water surface disturbances. A waiting period of at least 2 min followed any water perturbation before measurements were taken, ensuring minimum disturbance of the water surface.

The rolling spheres' velocity was determined by measuring the time it took to travel a fixed distance, with a minimum rolling distance of $20D$. This ensured that the spheres reached their time-mean terminal velocity prior to measurements. Initially, a stopwatch measured the time for a 200 mm distance on the removable panel (constituting 50% of data). Later, a system with three laser-based object detectors was introduced for improved accuracy and efficiency (50% of data). The results presented in this study incorporate both datasets and an uncertainty analysis presented in Nanayakkara *et al.* (2024b) addresses measurement errors from both methods. Sphere specifications are detailed in Table I. Data in Sec. V represent average measurements from eight separate runs using spheres of similar diameter and density.

TABLE I. Specifications of spheres used in this study. Each entry corresponds to a set of 8 individual spheres, with three measurements taken for each sphere. These spheres were also used in our previous study (Nanayakkara *et al.*, 2024b).

Sphere material	Sphere density $\rho_s (g/cm^3)$	Sphere diameter (mm)
Cellulose acetate	1.3	$6.35 \pm 0.03 \, (0.5\%)$
		$5.86 \pm 0.02 \, (0.3\%)$
		$4.87 \pm 0.03 \, (0.7\%)$
		$4.42 \pm 0.02 \, (0.5\%)$
		$3.94 \pm 0.02 \, (0.6\%)$
		$3.44 \pm 0.03 \, (0.8\%)$
Acrylic	1.2	$7.85 \pm 0.03 \, (0.4\%)$
		$6.33 \pm 0.03 \, (0.4\%)$
		$4.71 \pm 0.02 \, (0.4\%)$
		$3.95 \pm 0.07 \, (1.7\%)$

Occasional checks were conducted for randomly selected experimental parameters to confirm data consistency, even with variations in fluid temperature. Table I indicates that the uncertainty regarding sphere diameter was generally below 1%.

To prevent water absorption distortion, spheres and panels were regularly removed from the water tank outside measurement intervals and dried. Table I presents the uncertainty of sphere diameter for each set of spheres, measured by obtaining three distinct measurements of each of the ten spheres in a set. The uncertainty of sphere diameter was typically less than 1%. The uncertainty in sphere diameter was used to estimate deviations in sphericity. Given that the uncertainties in sphere diameter were generally below 1%, deviations in the sphericity of spheres were considered negligible. Preliminary experiments were conducted with a selection of spheres at various inclination angles ranging from 4° to 20° to examine potential sphere slippage in our experiments. A marker was placed on the surface of the sphere, and the sphere's rolling motion was recorded using a digital camera. The calculated rotational speed was compared to the measured linear down-slope velocity, revealing no significant difference between the two velocities (less than 1%). Therefore, any slippage between the sphere and the surface was deemed negligible.

To assess panel flatness, the surface height variation of the panel was measured at specific points, revealing that the panel's non-flatness was negligible (below 0.5%) compared to its downward slope (greater than 7%). Regular cleaning of the water tank prevented dust or fiber deposition on the panel surface.

Nanayakkara *et al.* (2024b) presented an uncertainty analysis of their experimental measurements. Since the same experimental setup was used for the results presented here, the same uncertainty values are applicable. As shown in Nanayakkara *et al.* (2024b), the bias error of measurements is approximately 1–2% for both $\overline{Re}$ and $\overline{C}_D$.

B. Surface roughness measurements

The surface roughness measurements of the panels were acquired using a KLA-Tencor D600 profiler located at the Australian Surface Metrology Lab (ASML) in Warrnambool, Victoria, Australia. ASML obtained these measurements on our behalf. The composite three-dimensional images shown in Fig. 2 were obtained by stitching together a minimum of 100 profile scans.

Many parameters are used to describe surface roughness, and they vary depending on the application. Amplitude parameters such as mean, root mean square (r.m.s.), or peak roughness that describe the vertical or amplitude characteristics of surface deviations are the most commonly used. Gadelmawla *et al.* (2002) discuss the analytical expressions that describe these parameters including some applications.

The measured panel roughness values are detailed in Table II. Three roughness parameters are shown in the table. R_q is the root mean square (r.m.s.) amplitude parameter. Additionally, we have indicated the skewness (R_{sk}) and kurtosis (R_{ku}) of each panel in Table II. Skewness measures the asymmetry of the surface profile: large positive skewness ($R_{sk} > 0.5$) indicates a higher percentage of peaks compared to valleys, large negative skewness ($R_{sk} < -0.5$) indicates a higher percentage of valleys compared to peaks and zero skewness indicates a symmetric distribution. Kurtosis measures the sharpness of the surface profile: high kurtosis ($R_{ku} > 3$) suggests sharp peaks and deep valleys (rougher texture), while low kurtosis ($R_{ku} < 3$) suggests a smoother

(a) Rough ceramic panel

(b) Rough glass 1 panel

(c) Rough glass 2 panel
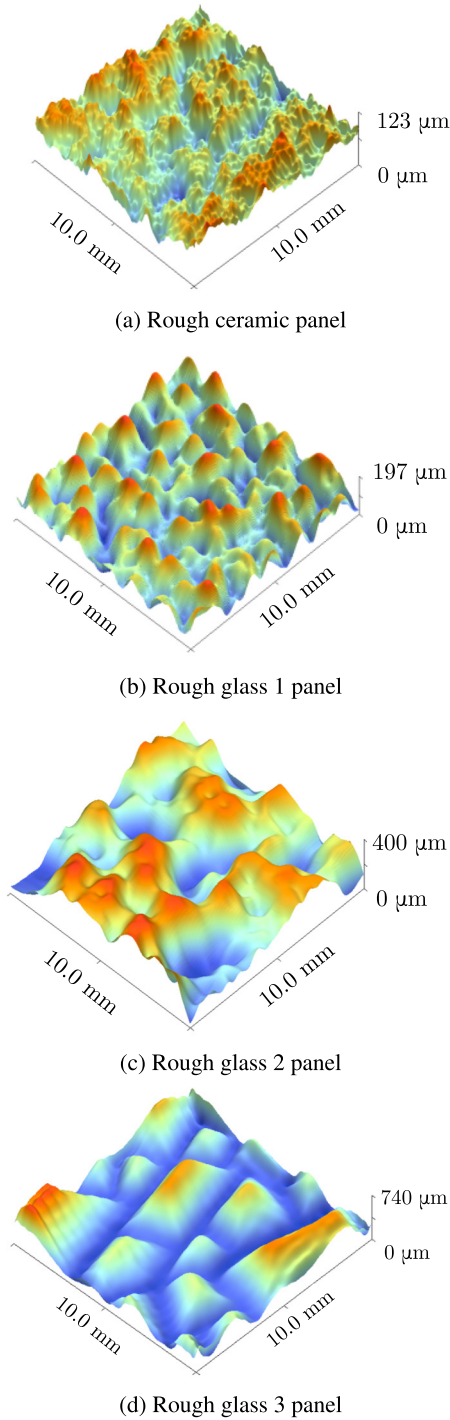

(d) Rough glass 3 panel

FIG. 2. Surface profiles of the rough panels. No waviness filtering was used.

texture with more rounded features. For the rough panels used in this study, we measured low kurtosis factors ($R_{ku} < 3$). This indicates that all four panels have an approximately symmetric distribution with rounded features with small R_{sk} for three of the four panels.

TABLE II. Surface roughness measurements of the four rough panels used in the present study. No waviness filtering was used. The measurement area was 100 mm².

Panel type	$R_q(\mu m)$	R_{sk}	R_{ku}
Rough ceramic	19.06	-0.26	2.55
Rough glass 1	39.36	0.10	2.24
Rough glass 2	97.05	-0.28	2.26
Rough glass 3	165.70	0.80	2.28

V. RESULTS AND DISCUSSION

This section presents the experimental results of the measured time-mean drag coefficients ($\overline{C}_D$) of spheres freely rolling on rough inclined panels. The drag coefficients for experimental measurements are determined using (5) and compared against the predicted drag coefficient as per (13). This section is structured as follows. First, we present the observed variations of $\overline{C}_D$ with $\overline{Re}$ for spheres rolling on the four rough panels in Sec. V A. Subsequently, the influence of the non-dimensional height of roughness (ξ_q) on $\overline{C}_D$ is discussed in Sec. V B. Furthermore, Sec. V C discusses the observed relationship between the coefficient of rolling resistance (μ_r) and surface roughness. In Sec. V D, the new model is proposed and in Sec. V E, measured drag values are compared against predicted values.

A. Measured $\overline{C}_D$ vs $\overline{Re}$ data

Using the experimental setup and methods detailed in Sec. IV, we acquired measurements of $\overline{C}_D$ vs $\overline{Re}$ within the range $30 < \overline{Re} < 800$. This involved testing 10 different diameter spheres on four distinct rough panels. Figure 3 displays all the collected data points, where the legend illustrates the marker shapes representing different sphere diameters and marker colors corresponding to the panel. The results of the same spheres tested on smoother panels presented in Nanayakkara *et al.* (2024b) are also shown in the same figure using light gray markers, for comparison.
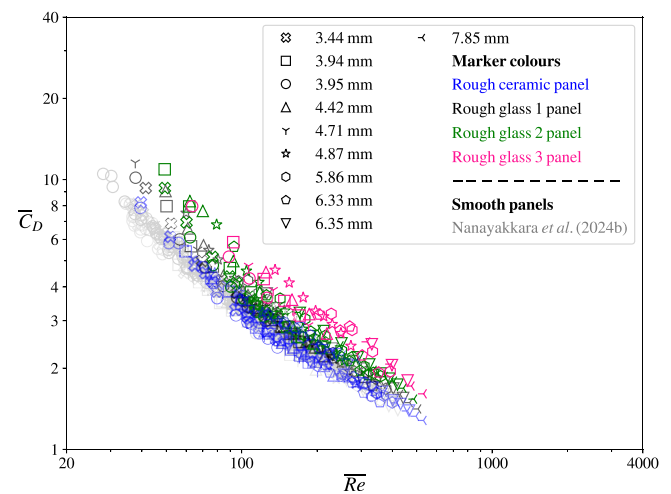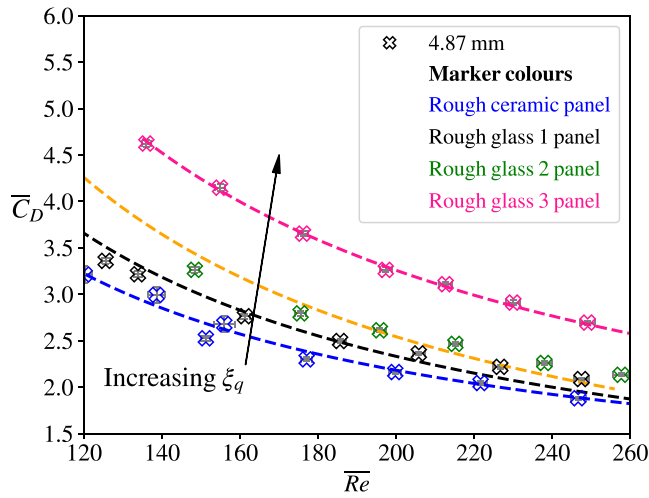

FIG. 3. $\overline{C}_D$ vs $\overline{Re}$ results of spheres rolling on rough panels. Smooth panel data from Nanayakkara *et al.* (2024b) are also shown for comparison.
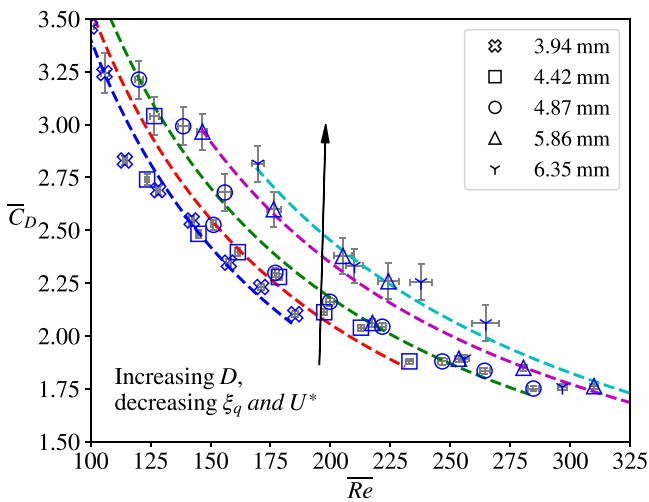
Comparing the $\overline{C}_D$ values of the present study against those discussed in Nanayakkara *et al.* (2024b), we see a clear increase in the measured values of $\overline{C}_D$ for the rougher panels. This trend is observed across all $\overline{Re}$ investigated. This observation implies that the increase in panel roughness induces a higher drag on the spheres, which we attribute to the added effects of rolling resistance due to the larger surface roughness of rough panels. Note that Nanayakkara *et al.* (2024b) found that the drag coefficient decreased as ξ_q was increased, consistent with the predicted lubrication fluid drag (10). The present study considers significantly rougher (10–100 times) surfaces than those investigated in Nanayakkara *et al.* (2024b).

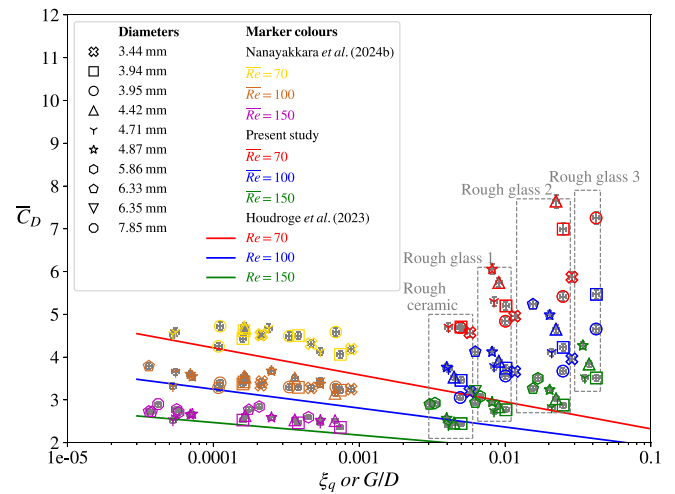Figure 4(a) highlights the increase in total drag with increasing panel roughness for a sphere with $D = 4.87$ mm, consistent with the present proposal. However, in Fig. 4(b), for a fixed panel roughness with sphere D varied, we observe an increase in drag with decreasing ξ_q (or increasing D). A similar observation was made in Nanayakkara *et al.* (2024b) for the fluid drag. However, given that ξ_q values for these rough panels are large, the lubrication drag is expected to be small. As such, this observed increase in the value of $\overline{C}_D$ with an increase in D for a fixed panel roughness is unlikely to be due to an increase in fluid drag. Therefore, Fig. 4 highlights that ξ_q and $\overline{Re}$ are insufficient to describe the contribution of rolling resistance to the total drag coefficient. In Sec. V D, it will be shown that this increase in drag with increasing D is likely due to an increase in non-dimensional velocity U^*, for a fixed $\overline{Re}$.

B. Measured $\overline{C}_D$ vs ξ_q data

Figure 5 shows the variation of $\overline{C}_D$ with ξ_q for the 4 rough panels considered at $\overline{Re} = 70, 100$, and 150. A linear interpolation technique was used to estimate the $\overline{C}_D$ values corresponding to each $\overline{Re}$. Error bars indicate the uncertainty of both R_q ($\approx 5\%$) and interpolated $\overline{C}_D$ ($\approx 2\%$) measurements. A degree of scatter is observed at each $\overline{Re}$; however, $\overline{C}_D$ is observed to generally increase with increasing ξ_q.

The results using the smooth panels presented by Nanayakkara *et al.* (2024b) are also shown in Fig. 5 to indicate the general trend. Combined analytical and numerical predictions of fluid drag from Eq. (10) are also shown in the figure as solid lines. The smooth panel data indicate that the measured and predicted drag coefficients decrease with increasing ξ_q up to $\xi_q \approx 0.001$. As the roughness is increased further ($\xi_q \geq 0.001$), we observe an increase in $\overline{C}_D$ corresponding to the rough panels.

For a fixed $\overline{Re}$, increasing ξ_q by increasing the panel roughness corresponds to an increase in the drag coefficient. However, $\overline{C}_D$ decreases when ξ_q is increased by decreasing D for a fixed panel (i.e.,

(a) $D = 4.87$ mm sphere on the four rough panels.

(b) Rough ceramic panel.

FIG. 4. Variation of $\overline{C}_D$ with $\overline{Re}$. Least squares lines of the form $a + b/Re$ have been fitted through data that correspond to the individual diameters of the spheres used. The coefficient of determination R^2 is typically ∼0.9. In Fig. 4(b), the arrow indicates the decrease in ξ_q and U^* corresponding to increasing D, at a fixed value of $\overline{Re}$.

FIG. 5. Variation of $\overline{C}_D$ with ξ_q at three fixed $\overline{Re}$. $\overline{C}_D$ values at specific $\overline{Re}$ values were calculated using linear interpolation of nearest neighbors. Gray dashed boxes are used to approximately indicate the data corresponding to each of the four panels. Results from smooth panels from Nanayakkara *et al.* (2024b) are also shown in the figure for comparison. C_D predictions from Eq. (10) are also plotted as solid lines for comparison with experimental results.

within each gray box). Therefore, increasing ξ_q by decreasing the sphere diameter results in a reduction in the drag coefficient while increasing ξ_q by increasing the panel roughness increases $\overline{C}_D$. A similar observation was made in Fig. 4. Therefore, we highlight that ξ_q alone is insufficient to explain the observed variation in the total drag coefficient. Figures 4 and 5 highlight that the drag due to rolling resistance does not scale with $\overline{Re}$, and a new non-dimensional velocity U^* is required to describe the velocity dependence of the coefficient of rolling resistance.

The observed increase in $\overline{C}_D$ for a fixed panel with decreasing ξ_q by increasing D, at a fixed $\overline{Re}$, is likely due to a variation of U^*. For example, at $\overline{Re} = 100$, varying D from $D = 3.44$ mm to $D = 4.87$ mm results in an approximate change of U^* between 0.16 and 0.09, respectively, which is an approximately 44% reduction of U^*.

Furthermore, $\overline{Re}$ has a decreasing effect on $\overline{C}_D$. As $\overline{Re}$ is increased from 70 to 150, we observed a significant reduction in measured $\overline{C}_D$, from $\overline{C}_D \approx 7$ to $\overline{C}_D \approx 3$, an approximate 60% reduction in mean value across all D.

To establish the effects of the roughness on the drag caused by rolling resistance, Fig. 6 investigates the dependence of $\overline{C}_{D,\text{rr}}$ on U^* and ξ_q. $\overline{C}_{D,\text{rr}}$ was calculated using the following equation:

$$\overline{C}_{D,\text{rr}} = \overline{C}_{D,\text{exp}} - \overline{C}_{D,\text{f,eff}}. \tag{18}$$

Figure 6(a) compares the $\overline{C}_{D,\text{rr}}$ variation with U^* for a sphere of $D = 4.87$ mm rolling on the four panels. Here, the effects of increasing ξ_q by increasing panel roughness on $\overline{C}_{D,\text{rr}}$ is highlighted, as D is fixed. Figure 6(b) indicates the $\overline{C}_{D,\text{rr}}$ vs U^* relationship for the panel Rough glass 3, with the sphere D varied. Again, we observed that $\overline{C}_{D,\text{rr}}$ increases with increasing ξ_q created by a smaller D. Least squares lines of the form $a(U^*)^b$ have been fitted through the data for a fixed ξ_q in both figures with R^2 values typically ~ 0.9. The figures clearly show the increase in $\overline{C}_{D,\text{rr}}$ with increasing panel roughness R_q or decreasing D. Therefore, Fig. 6 shows that the behavior of $\overline{C}_{D,\text{rr}}$ is captured well with ξ_q and U^*. Figure 6 also highlights the decreasing behavior of $\overline{C}_{D,\text{rr}}$ with increasing U^* for a fixed value of ξ_q.

C. Relationship between μ_r and surface roughness

In Sec. III, we proposed a new model to describe the coefficient of rolling resistance, which takes the form $\mu_r = a \times (\xi_q)^b \times (U^*)^c$, where a, b, and c are constants to be determined empirically. In this section, we will determine suitable values for the constants, which capture the relative contribution of each variable to effectively describe μ_r.

First, we will define $\mu_{r,\text{eff}}$ as the effective μ_r required to match the predictions of Eq. (13) with the experimental measurements. Here, we have used R_q of the panels as an approximation for the gap height G required for Eq. (10). $\mu_{r,\text{eff}}$ is calculated as follows:

$$\mu_{r,\text{eff}} = \frac{\overline{C}_{D,\text{exp}} - \overline{C}_{D,\text{f,eff}}}{4D(\beta - 1)g\cos(\theta)/3\overline{U}^2}. \tag{19}$$

We note that the data points for $\overline{Re} > 300$ were excluded from this analysis, since (10) is only valid in the range $5 < Re < 300$. $\mu_{r,\text{eff}}$ will be used to calculate the constants in Eq. (16).

D. New empirical model for the coefficient of rolling resistance

Least squares regression analysis was conducted on the derived $\mu_{r,\text{eff}}$ values for all the data for the four panels, and an equation of the
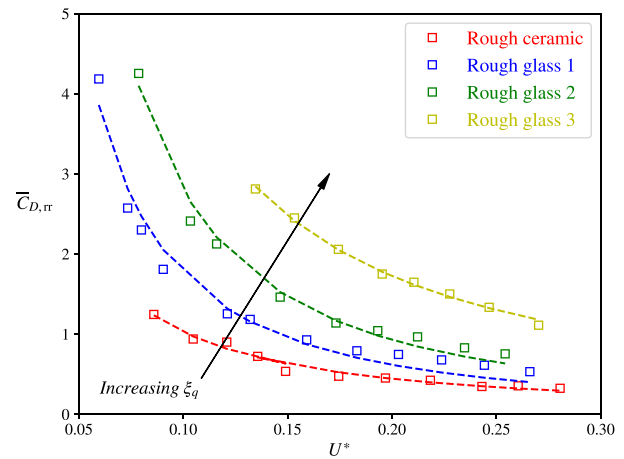

(a) Four panels with a fixed D =4.87 mm
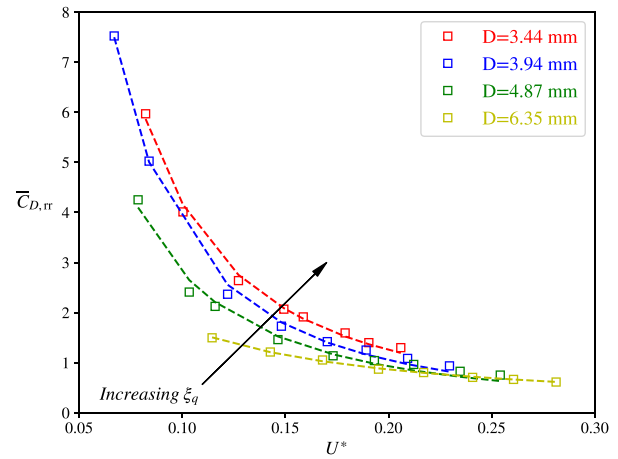
(b) Four spheres for panel Rough glass 3 with a fixed Rq

FIG. 6. Variation of $\overline{C}_{D,\text{rr}}$ with U^*. Least squares lines of the form $a(U^*)^b$ have been plotted through the data corresponding to each panel with R^2 values typically 0.9.

form $\mu_{r,\text{pred}} = a(\xi_q)^b(U^*)^c$ has been fitted through the data. Based on this regression analysis, coefficients that minimize the residuals were derived and the following equation was obtained:

$$\mu_{r,\text{pred}} = 5 \times (\xi_q)^{0.7}(U^*)^{0.6}. \tag{20}$$

In Fig. 7, we compare the calculated $\mu_{r,\text{eff}}$ against values predicted using the proposed model (20). The new model demonstrates a strong predictive capability, as evidenced by the coefficient of determination (R^2) value of approximately 0.9. This high R^2 value indicates that approximately 90% of the variance in the measured values is explained by the model, suggesting good alignment between the predicted and actual data points. The scatterplot in Fig. 7, which compares measured values against the model's predictions, shows that the predictions closely follow the ideal fit line (solid black line), reinforcing the model's accuracy, with a minor divergence as noted at large values $\mu_{r,\text{eff}}$. Such performance highlights the model's robustness and reliability in predicting $\mu_{r,\text{eff}}$.
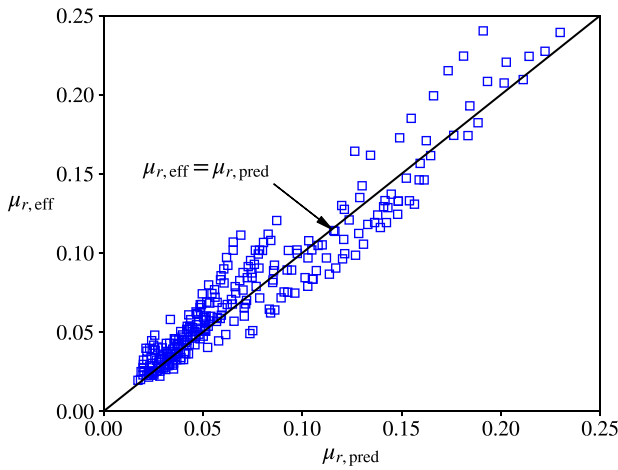
FIG. 7. Comparison of $\mu_{r,\text{eff}}$ with $\mu_{r,\text{pred}}$ based on least squares regression analysis. $R^2 = 0.90$ indicates a good fit between measured and predicted values.

Equation (20) suggests the non-linear power-law dependence on both ξ_q and U^*. This is in general agreement with non-linear dependence on roughness and velocity observed by previous investigations (Cross, 2015, 2016).

Furthermore, Eq. (17) can be re-written using the new model for $\mu_{r,\text{pred}}$ as

$$\overline{C}_{D,rr} = \frac{20 \times (\xi_q)^{0.7} \times (\beta - 1)\cos\theta}{3(U^*)^{1.4}}. \tag{21}$$

In Fig. 4(b), we observed an increase in total drag with decreasing ξ_q and U^* for a fixed $\overline{Re}$. This observation can be explained using (21). Increasing D has a twofold effect on $\overline{C}_{D,rr}$. First, the decrease in ξ_q decreases $\overline{C}_{D,rr}$ with a $\xi_q^{0.7}$ dependence. Second, however, the decrease in U^* causes an increase in $\overline{C}_{D,rr}$ with a $(U^*)^{1.4}$. Therefore, U^* has a stronger effect on $\overline{C}_{D,rr}$, which leads to the observed increase in total drag in Fig. 4, at a fixed $\overline{Re}$.

E. Comparison of measured $\overline{C}_D$ vs $\overline{Re}$ data against new rolling resistance model

In Fig. 8, we compare the measured $\overline{C}_D$ with the $\overline{C}_{D,\text{pred}}$ given in Eq. (13), including the contribution of rolling resistance characterized by Eq. (20). The fluid drag predictions from Eq. (10) are also plotted in the figures as a cyan dashed line for comparison. The sphere diameter was kept constant ($D = 4.87$ mm) to enable effective comparison of the influence of panel roughness on $\overline{C}_D$. The figure shows that Eq. (13) provides a good approximation of the measured total drag for all four panels. The combined drag coefficient follows the same trend and matches the varying roughness between the panels. The figure shows that the proposed model has captured the general trend in behavior with good accuracy.

Figure 9 shows the $\overline{C}_D$ vs ξ_q plots with sphere $D \approx 4$ mm at three values of $\overline{Re}$ (70, 100, and 150). The combined drag coefficient including rolling resistance is also shown in the figure. We observe that the new model captures the increasing $\overline{C}_D$ for rougher panels, in good agreement with experimental data.

Therefore, Figs. 8 and 9 together with Fig. 7 support our proposal that rolling resistance is dependent on ξ_q and the sphere non-dimensional velocity U^*. The coefficients calculated using the regression approach give consistent predictions of the coefficient of rolling resistance, which compares well when considered as a drag coefficient. The increase in panel roughness induces a larger resistive force, which scales ξ_q to the power of 0.7.
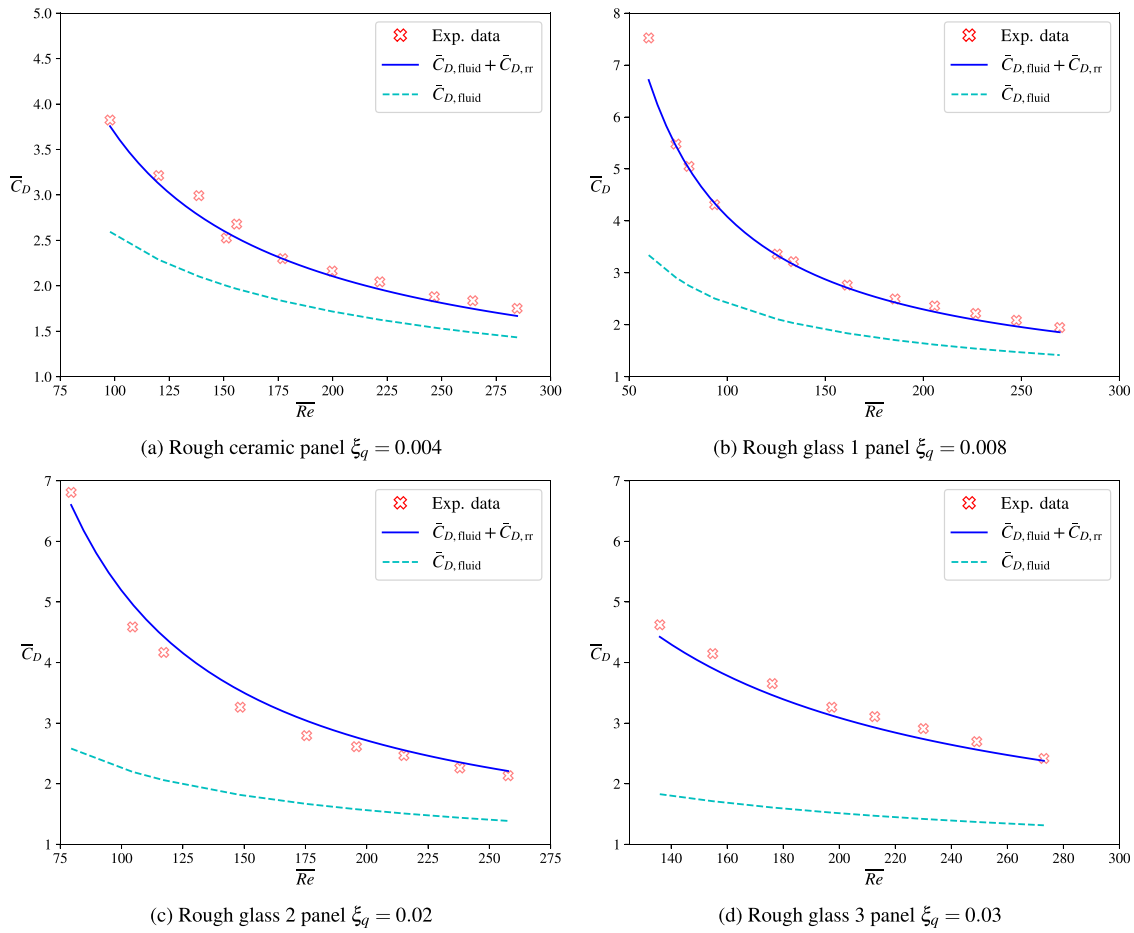
Increasing panel roughness affects the drag coefficient in two main ways. First, as R_q increases, the fluid drag decreases because the imposed gap grows, reducing lubrication drag in the gap region. However, higher panel roughness also leads to greater drag from rolling resistance, which also depends on R_q. Rougher panels increase the coefficient of rolling resistance, resulting in higher drag forces. Notably, when the surface roughness is sufficiently large, the rise in rolling resistance outweighs the reduction in fluid drag for a given roughness, leading to an overall increase in total drag with increasing panel roughness.

In the present study, we have obtained a $\mu_r \propto 1/D$ dependence, in general agreement with the experimental observations made by Cross (2016). However, our analysis suggests a $\mu_r \propto U^{0.6}$, in disagreement with the results of Cross (2016). This difference in the velocity dependence between the two studies is likely due to the exclusion of aerodynamic drag by Cross (2016) in their derivation of μ_r. Wilson et al. (2017) proposed a rolling resistance model with $\mu_r \propto U^2/D$. Although the same D dependence was observed here, we observed a $U^{0.6}$ as opposed to the proposed U^2 behavior. As such, it is likely that either $\hat{\hat{\xi}}$, η_n, and $n_{2\pi}$ or a combination of these parameters is dependent on U.

1. Model limitations

We note that this model is only valid for the range of experimental parameters investigated in this study. That is, $0.002 < \xi_q < 0.05$ and $0.03 < U^* < 0.3$.

Nanayakkara et al. (2024b) discuss the influence of the distribution of asperities, which has a significant impact on the imposed gap height between a sphere and the plane. Similarly, we expect that the surface finish will significantly affect the rolling resistance on a rolling sphere. As discussed in Sec. IV B, the four panels used in this study had an approximately symmetric distribution of asperities with rounded features (small skewness with a small < 3 kurtosis factor). When the surface texture deviates from this, and possibly for highly skewed surfaces with sharp features or highly structured surfaces, the rolling resistance may behave differently. The development of a resistance model that is valid for all types of roughness is challenging as the mode of energy loss through contact will differ with varying surface characteristics. One example is as roughness is increased further, contact with a large asperity leads to sphere liftoff. Then, the sphere is airborne and makes contact with the surface again due to gravity. In this scenario, rolling resistance does not act on the sphere while airborne and the effective drag will not be described effectively from the model we have presented here. Development of a rolling resistance model that includes larger scales of roughness will require the collection of data from a broader range of surfaces, which is beyond the scope of the present investigation. However, we expect that for different surface textures, the dependence on roughness and velocity will remain consistent with different power-law behaviors.

(a) Rough ceramic panel $\xi_q = 0.004$

(b) Rough glass 1 panel $\xi_q = 0.008$

(c) Rough glass 2 panel $\xi_q = 0.02$

(d) Rough glass 3 panel $\xi_q = 0.03$

FIG. 8. Comparison of measured drag coefficient against model predictions for a CA sphere with $D = 4.87$ mm rolling on the four rough panels. The solid blue line shows the $\overline{C}_{D,\text{pred}}$. Cyan dashed line indicates the $\overline{C}_{D,\text{f}}$ given by Eq. (10).

We acknowledge that it is possible that other measures of roughness can be used instead of R_q that may also capture the distribution of asperities. Since many roughness statistics are available, the investigation of other parameters was considered beyond the scope of this investigation. We aimed to demonstrate that surface roughness is a likely source of rolling resistance for hard spheres rolling on hard surfaces, which we have shown using the simple R_q parameter. We recommend the investigation of other roughness parameters in future work.

## VI. OTHER SOURCES OF ROLLING RESISTANCE

Rolling resistance is a complex phenomenon that may involve many mechanisms as introduced in Sec. I. We have proposed that surface roughness is a primary parameter that determines the rolling resistance of hard spheres on a hard surface. However, additional mechanisms of rolling resistance have been presented in previous investigations. We shall discuss some of these mechanisms here in more detail.

One mechanism responsible for the rolling resistance of spheres is bulk deformation. Brilliantov and Pöschel (1998) presented a

first-principles expression for the rolling friction coefficient of a visco-elastic sphere rolling on a hard plane. They assumed that surface effects are negligible and attributed deformation due to viscous dissipation in the material as the primary source of rolling friction. Their expressions use material and viscous constants to predict a frictional torque. Brilliantov and Pöschel (1999) used this approach to calculate the rolling resistance of a rolling sphere, assuming the resistance is due to energy losses associated with continuous viscoelastic collisions. They found that the coefficient of rolling friction is proportional to the sphere velocity and a material constant that depends on the coefficient of restitution, and presented the following relationship:

$$\mu_{roll} = \frac{U(1-\varepsilon)}{2.28(\rho/m)^{2/5}\overline{g}^{1/5}}, \qquad (22)$$

where ε is the coefficient of restitution, $\rho = Y\sqrt{D}/(3(1-\nu))$ where Y is the Young modulus and ν the Poisson ratio, and m is the mass of the sphere. $\overline{g}$ is the initial relative sphere velocity. We note that μ_{roll} in Eq. (22) is similar to d with dimension of length. To compare with our results, it was non-dimensionalized as $\mu_{roll}/(D/2)$. The predicted $\mu_{roll}/(D/2)$ values using the Brilliantov and Pöschel (1999) model for
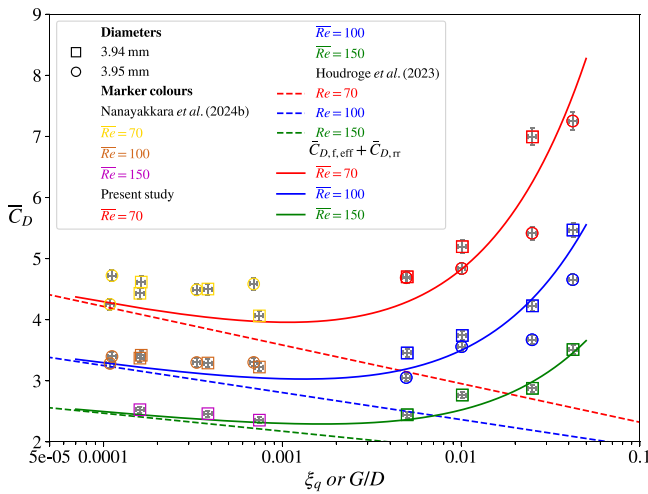
FIG. 9. Variation of $\overline{C}_D$ with ξ_q at three fixed $\overline{Re}$ for $D \approx 4$ mm spheres. $\overline{C}_D$ values at specific $\overline{Re}$ values were calculated using linear interpolation of nearest neighbors. Results from smooth panels from Nanayakkara *et al.* (2024b) are also shown. C_D predictions from Eq. (10) are also plotted as dashed lines. The new model proposed in Eq. (13) is represented by solid lines.

our spheres with $\varepsilon = 0.9$ and $\overline{g} = U$ are smaller ($\approx 10^{-5}$ times) compared to the measured μ_{eff} values of the present study. This suggests that viscoelastic collisions make negligible contribution to our spheres. However, for soft spheres rolling on a hard surface, the viscoelastic effects may be significant.

Contact plasticity or plastic deformation is another mechanism that is generally applicable to soft materials that are easily deformed. The rolling sphere or surface is permanently deformed, which leads to an additional resistive torque. Eldredge and Tabor (1955) have observed that repeated rolls of a steel ball over the same surface of a softer metal lead to a reduction in the measured coefficient of rolling resistance. For the hard spheres (acrylic and cellulose acetate) rolling on hard surfaces (glass and ceramic), we can assume that contact plasticity does not affect the rolling motion in the present investigation.

Particle shape has also been found to influence the rolling resistance of spheres (Wensrich and Katterfeld, 2012). Deviations from sphericity may introduce additional resistivity to rotational motion, which may be further emphasized by an increase in asymmetric contact. Similarly, d'Ambrosio *et al.* (2023), investigating the rheology of suspensions, found an increase in the coefficient of rolling resistance for particles with flat surfaces (large regions of the surface are non-spherical) compared to spherical particles. Since the deviations from sphericity for the spheres used in the present study are small, particle shape effects are also assumed to be negligible.

Interfacial slip was proposed by Reynolds (1876) as another source of rolling resistance, by conducting experiments using rubber rollers. The work of Sharma and Reid (1999) presents a thorough review of the history of interfacial slip while also providing a discussion on the role of interfacial slip on the rolling resistance of spheres. They propose a state of motion of the sphere termed quasi-rolling, where the velocity of the contact point becomes zero while sliding slowly at varying speeds. The equilibrium condition under which quasi-rolling occurs is given by Eq. (11), where the normal contact force is shifted to

the forward direction from the midpoint, denoted as d. They propose that to maintain zero velocity at the point of contact, a rolling friction force must exist, to maintain the no-slip boundary condition. However, since the value of d is unknown, their model is incomplete.

Finally, particle adhesion is another mechanism that has been proposed to lead to rolling resistance. The energy dissipation associated with the breaking of adhesive bonds as the particle leaves contact leads to a resistance to rolling (Dominik and Tielens, 1995; Wilson *et al.*, 2017). However, adhesive forces are significant in particles with small diameters such as fine powders. Therefore, we expect adhesive forces to be negligible for our spheres.

For a sphere rolling without slipping on a given surface, the mechanism that dominates the rolling resistance will be a function of sphere and panel properties. However, it is likely that a combination of mechanisms discussed above will act on the sphere, while some mechanisms may dominate over others. For hard spheres rolling on a hard surface, we expect surface roughness to be the primary mechanism that leads to rolling resistance. Since all mechanisms act through the contact area between the sphere and the plane, and contact occurs through surface roughness, the contribution of other mechanisms will also indirectly depend on surface roughness.

VII. INFLUENCE OF PANEL ROUGHNESS ON SPHERE WAKE

The wake of a freely rolling sphere is complex and dependent on $\overline{Re}$. Nanayakkara *et al.* (2024b) discuss the influence of $\overline{Re}$ on sphere wake shedding and vortex-induced vibrations (VIVs). At low $\overline{Re}$, the wake is steady and with increasing $\overline{Re}$, the frequency of shedding increases, and the wake becomes highly chaotic at larger $\overline{Re}$. For the relatively smooth surfaces investigated by Nanayakkara *et al.* (2024b), no direct influence of surface roughness on the sphere wake characteristics was observed. However, the influence of large roughness on the sphere wake has not been investigated previously.

To establish the effects of surface roughness on the sphere wake, visualizations of a sphere with the same diameter rolling on panels with different surface roughnesses were obtained at a similar $\overline{Re}$. Figure 10 shows the wake of a sphere rolling on two relatively smooth Nanayakkara *et al.* (2024b) and three rough panels. The corresponding ξ_q values of the panels as well as $\overline{Re}$ and measured Strouhal number, $St = fD/\overline{U}$, where f is the vortex shedding frequency, are indicated in the caption of each figure. The $\overline{Re}$ values of the rolling spheres are approximately the same to enable effective comparison of the effects of surface roughness on the spheres' wake dynamics.

As observed in Fig. 10, the wake of spheres rolling on the glass and frosted glass panels displays a high degree of similarity, and the St values are also nearly identical. The sphere rolls down in a straight line with some minor fluctuations in the cross-slope displacement caused by the shedding of hairpin vortices. Nanayakkara *et al.* (2024b) presents a detailed investigation of the influence of vortex shedding on the sphere displacement and cross-slope velocity.

However, for the rough ceramic panel, a marginal increase in wake unsteadiness is observed characterized by increase in the frequency of vortex shedding and the corresponding St. When the panel roughness is increased further, this unsteadiness amplifies, leading to an increased frequency of vortex shedding and significant cross-slope oscillations. The increased panel roughness has led to the wake being significantly chaotic, at a lower $\overline{Re}$ compared to the smoother panels.
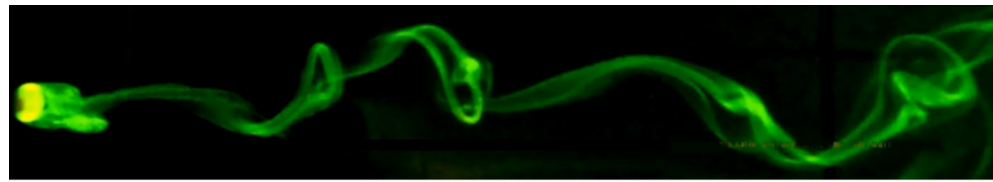
(a) Glass panel ($\xi_q = 4.5 \times 10^{-6}$) at $\overline{Re} = 174(\pm 2)$, $St = 0.11$
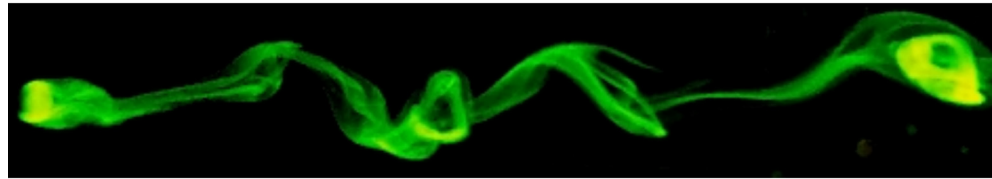
(b) Frosted glass panel ($\xi_q = 0.0004$) at $\overline{Re} = 175(\pm 2)$, $St = 0.10$
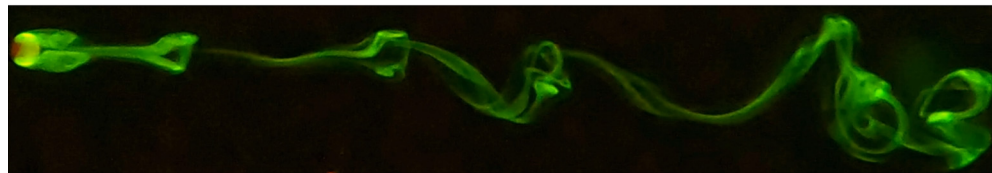
(c) Rough ceramic panel ($\xi_q = 0.003$) at $\overline{Re} = 174(\pm 2)$, $St = 0.15$
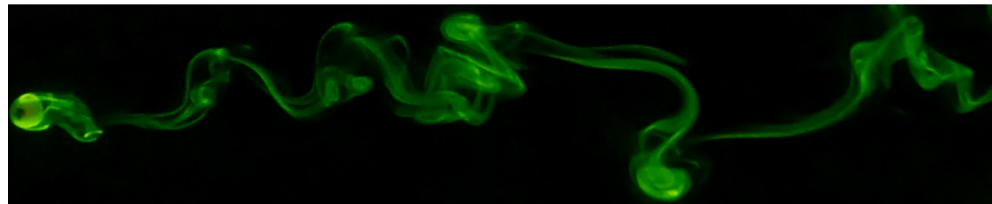
(d) Rough glass 2 panel ($\xi_q = 0.015$) at $\overline{Re} = 180(\pm 2)$, $St = 0.30$
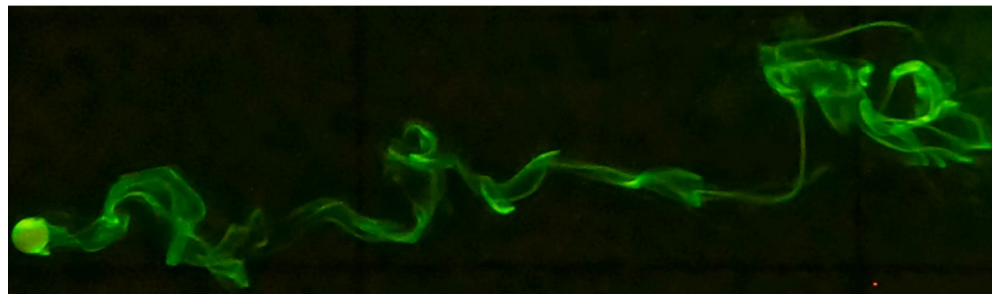
(e) Rough glass 3 panel ($\xi_q = 0.026$) at $\overline{Re} = 178(\pm 2)$, $St \approx 0.32$

FIG. 10. Plan view of a sphere of $D = 6.35$ mm rolling on different panels at similar $\overline{Re}$. The effects of increasing surface roughness on the wake of a rolling sphere are highlighted in this figure. The sphere is rolling from right to left.

A level of unsteadiness similar to that shown in Fig. 10(e) was observed at $\overline{Re} \approx 700$ by Nanayakkara *et al.* (2024b). Therefore, based on the flow visualizations presented here, surface roughness acts to accelerate the onset of unsteadiness of the wake of the rolling sphere. This roughness effect appears to be independent of $\overline{Re}$ and increases with increasing panel roughness.

One possibility is that this increase in unsteadiness is caused by collisions with surface asperities when the sphere is rolling down the plane, which leads to instantaneous change in the rolling directions.

However, to quantify this effect, it is necessary to measure the change in sphere motion caused by collisions with large asperities. It is a challenging task to obtain such measurements due to scale separations between the two geometries; roughness in the micrometer length scale while wake shedding occurs in a millimeter length scale. Additionally, there are difficulties in effectively capturing the contact region of a moving sphere. Such an analysis is beyond the scope of the present investigation and we propose this as future work. Here, we have qualitatively shown the influence of surface roughness on the wake

shedding of a freely rolling sphere, with a significant increase in wake unsteadiness observed for larger roughness.

VIII. CONCLUSION

This study examines the drag coefficient (C_D) of a sphere rolling freely without slipping down a rough inclined plane. The effects of sphere time-mean Reynolds number ($\overline{Re}$) on the measured time-mean drag coefficient ($\overline{C}_D$) are discussed with respect to panel roughness. Lubrication theory (Goldman *et al.*, 1967; Houdroge *et al.*, 2023) predicts a decreasing C_D with increasing gap height or surface roughness. However, the findings of this study indicate that the $\overline{C}_D$ for a sphere increases with increasing roughness, in contradiction to lubrication theory. We suggest that this increase in $\overline{C}_D$ is due to the added effects of rolling resistance, which increases with roughness.

Due to the lack of an analytical or numerical model that effectively describes the relationship between the coefficient of rolling resistance (μ_r) with surface roughness, an empirical approach is used. A new model for the coefficient of rolling resistance $\mu_r = a(\xi_q)^b(U^*)^c$ is proposed. ξ_q is the non-dimensional r.m.s. roughness, U^* is the non-dimensional down-slope velocity, and a, b, and c are constants to be determined empirically. Analysis of the $\mu_{r,\text{eff}}$ data collected suggests that the equation $\mu_{r,\text{pred}} = 5(\xi_q)^{0.7}(U^*)^{0.6}$ provides accurate predictions of the total drag on a rolling sphere. The $\mu_{r,\text{pred}}$ values were compared against $\mu_{r,\text{eff}}$ data, with $R^2 \simeq 0.9$ suggesting that the proposed model effectively explains the variance of the measured data.

The increasing panel roughness ξ_q has a twofold effect on the drag coefficient. First, the fluid drag decreases due to increasing gap height. However, the drag due to rolling resistance increases. The increase in rolling resistance drag is larger than the decrease in fluid drag, for a given roughness, and we observed an increase in total drag with increasing panel roughness.

These findings may be useful in optimizing the performance and efficiency of small ball and roller bearings. The total resistance or drag can be minimized by selecting the appropriate surface finish for the bearings and the wall while also effectively understanding the effects of wear over time.

Experimental flow visualizations indicate that a higher panel roughness leads to a more chaotic wake compared to smoother panels at similar $\overline{Re}$. The Strouhal numbers St at similar $\overline{Re}$ were similar for the smoother panels, and they increased significantly for the rougher panels, highlighting this trend.

The relationship between rolling resistance and surface roughness is complex and is not yet fully understood. The present analysis provides an approximate model that requires the determination of parameters empirically based on experimental measurements. Measurement of the contact dynamics of spheres and roughness elements will be required to gain further insight into this problem. The combination of surface roughness with other sources of rolling resistance is likely to produce a more complete model that describes the dynamics of rolling spheres.

AUTHOR DECLARATIONS
Conflict of Interest

The authors have no conflicts to disclose.

Author Contributions

S. D. J. S. Nanayakkara: Conceptualization (equal); Data curation (equal); Formal analysis (equal); Investigation (equal); Methodology (equal); Validation (equal); Visualization (equal); Writing – original draft (equal); Writing – review & editing (equal). **S. J. Terrington:** Conceptualization (equal); Methodology (equal); Supervision (equal); Writing – review & editing (equal). **J. Zhao:** Conceptualization (equal); Funding acquisition (equal); Project administration (equal); Supervision (equal); Writing – review & editing (equal). **M. C. Thompson:** Conceptualization (equal); Funding acquisition (equal); Project administration (equal); Resources (equal); Supervision (equal); Writing – review & editing (equal). **K. Hourigan:** Conceptualization (equal); Funding acquisition (equal); Project administration (equal); Resources (equal); Supervision (equal); Writing – review & editing (equal).

DATA AVAILABILITY

The data that support the findings of this study are available from the corresponding author upon reasonable request.

REFERENCES

Ai, J., Chen, J. F., Rotter, J. M., and Ooi, J. Y., "Assessment of rolling resistance models in discrete element simulations," Powder Technol. **206**, 269–282 (2011).

Bikerman, J. J., "Effect of surface roughness on rolling friction," J. Appl. Phys. **20**, 971–975 (1949).

Brilliantov, N. V. and Pöschel, T., "Rolling friction of a viscous sphere on a hard plane," Europhys. Lett. **42**, 511 (1998).

Brilliantov, N. V. and Pöschel, T., "Rolling as a 'continuing collision'," Eur. Phys. J. B **12**, 299–301 (1999).

Carty, J., "Resistance coefficients for spheres on a plane boundary," B.Sc. thesis (Massachusetts Institute of Technology, Department of Civil and Sanitary Engineering, Cambridge, 1957).

Cross, R., "Effects of surface roughness on rolling friction," Eur. J. Phys. **36**, 065029 (2015).

Cross, R., "Coulomb's law for rolling friction," Am. J. Phys. **84**, 221–230 (2016).

Dominik, C. and Tielens, A. G. G. M., "Resistance to rolling in the adhesive contact of two elastic spheres," Philos. Mag. A **72**, 783–803 (1995).

d'Ambrosio, E., Koch, D. L., and Hormozi, S., "The role of rolling resistance in the rheology of wizarding quidditch ball suspensions," J. Fluid Mech. **974**, A36 (2023).

Eldredge, K. R. and Tabor, D., "The mechanism of rolling friction. I. The plastic range," Proc. R. Soc. A **229**, 181–198 (1955).

Gadelmawla, E. S., Koura, M. M., Maksoud, T. M. A., Elewa, I. M., and Soliman, H. H., "Roughness parameters," J. Mater. Process. Technol. **123**, 133–145 (2002).

Galvin, K. P., Zhao, Y., and Davis, R. H., "Time-averaged hydrodynamic roughness of a noncolloidal sphere in low Reynolds number motion down an inclined plane," Phys. Fluids **13**, 3108–3119 (2001).

Garde, R. J. and Sethuraman, S., "Variation of the drag coefficient of a sphere rolling along a boundary," La Houille Blanche **55**, 727–732 (1969).

Goldman, A. J., Cox, R. G., and Brenner, H., "Slow viscous motion of a sphere parallel to a plane wall—I Motion through a quiescent fluid," Chem. Eng. Sci. **22**, 637–651 (1967).

Halling, J., "The relationship between surface texture and rolling resistance of steel," Br. J. Appl. Phys. **9**, 421 (1958).

Houdroge, F. Y., Zhao, J., Terrington, S. J., Leweke, T., Hourigan, K., and Thompson, M. C., "Fluid–structure interaction of a sphere rolling along an inclined plane," J. Fluid Mech. **962**, A43 (2023).

Hutchings, I. M., "Leonardo da Vinci's studies of rolling-element, disc and sector bearings," Proc. Inst. Mech. Eng., Part J **238**, 372 (2023).

Jan, C. D. and Chen, J. C., "Movements of a sphere rolling down an inclined plane," J. Hydraul. Res. **35**, 689–706 (1997).

Jan, C. D. and Shen, H. W., "Drag coefficients for a sphere rolling down an inclined channel," J. Chin. Inst. Eng. **18**, 493–507 (1995).

King, M. R. and Leighton, Jr., D. T., "Measurement of the inertial lift on a moving sphere in contact with a plane wall in a shear flow," Phys. Fluids **9**, 1248–1255 (1997).

Nanayakkara, S., Zhao, J., Terrington, S., Thompson, M., and Hourigan, K., "Effects of surface roughness on the drag coefficient of finite-span cylinders freely rolling on an inclined plane," J. Fluid Mech. (to be published) (2024a).

Nanayakkara, S., Zhao, J., Terrington, S., Thompson, M., and Hourigan, K., "Effects of surface roughness on the drag coefficient of spheres freely rolling on an inclined plane," J. Fluid Mech. **984**, A13 (2024b).

Reynolds, O., "VI. On rolling-friction," Philos. Trans. R. Soc. London **166**, 155–174 (1876).

Sharma, N. L. and Reid, D. D., "Rolling as a frictional equilibration of translation and rotation," Eur. J. Phys. **20**, 129 (1999).

Smart, J. R., Beimfohr, S., and Leighton, Jr., D. T., "Measurement of the translational and rotational velocities of a noncolloidal sphere rolling down a smooth inclined plane at low Reynolds number," Phys. Fluids **5**, 13–24 (1993).

Smart, J. R. and Leighton, Jr., D. T., "Measurement of the hydrodynamic surface roughness of noncolloidal spheres," Phys. Fluids **1**, 52–60 (1989).

Sun, Z., Premarathna, W. A. A. S., Anupam, K., Kasbergen, C., and Erkens, S. M. J. G., "A state-of-the-art review on rolling resistance of asphalt pavements and its environmental impact," Constr. Build. Mater. **411**, 133589 (2024).

Tabor, D., "The mechanism of rolling friction II. The elastic range," Proc. R. Soc. London, Ser. A **229**, 198–220 (1955).

Thompson, M. C., Leweke, T., and Hourigan, K., "Bluff bodies and wake–wall interactions," Annu. Rev. Fluid Mech. **53**, 347–376 (2021).

Wensrich, C. M. and Katterfeld, A., "Rolling friction as a technique for modelling particle shape in DEM," Powder Technol. **217**, 409–417 (2012).

Wilson, R., Dini, D., and Van Wachem, B., "The influence of surface roughness and adhesion on particle rolling," Powder Technol. **312**, 321–333 (2017).

Zhao, Y., Galvin, K. P., and Davis, R. H., "Motion of a sphere down a rough plane in a viscous fluid," Int. J. Multiphase Flow **28**, 1787–1800 (2002).

15 October 2024 06:34:02